Supplementary material of "A ferromagnetic Eu-Pt surface compound grown below hexagonal boron nitride"

Alaa Mohammed Idris Bakhit[1,2]**, Khadiza Ali**[3,4]**, Anna A. Makarova**[5]**, Igor Píš**[6]**, Federica Bondino**[6]**, Roberto Sant**[7]**, Saroj P. Dash**[4]**, Rodrigo Castrillo**[1]**, Yuri Hasegawa**[1,8]**, J. Enrique Ortega**[1,2,3]**, Laura Fernandez**[1]**, and Frederik Schiller**[1,3]

[1] Centro de Física de Materiales CSIC-UPV/EHU-Materials Physics Center, E-20018 San Sebastián, Spain

[2] Departamento de Física Aplicada I, Universidad del País Vasco UPV/EHU, E-20018 San Sebastián, Spain

[3] Donostia International Physics Center, E-20018 Donostia-San Sebastián, Spain

[4] Chalmers University of Technology, Göteborg, Chalmersplatsen 4, 412 96 Göteborg, Sweden

[5] Physikalische Chemie, Institut für Chemie und Biochemie, Freie Universität Berlin, Arnimallee 22, 14195 Berlin, Germany

[6] IOM-CNR, Strada Statale 14 Km 163.5, I-34149 Trieste, Italy

[7] ESRF, The European Synchrotron, 71 Avenue des Martyrs, CS40220, 38043 Grenoble Cedex 9, France

[8] Department of Physical Sciences, Ritsumeikan University, Kusatsu, 525-8577, Japan

E-mail: frederikmichael.schiller@ehu.es

The supplementary information file contains:

Supplementary Figures S1-S8

Supplementary information and data are provided to further illustrate the intercalation process of Eu below the hBN/Pt substrate as well as magnetic easy axis determination of the Eu-Pt alloy below hBN.

S1. Spectroscopy analysis of insufficient temperature for Eu intercalation

Eu does not completely intercalate below a hBN layer on Pt if the substrate temperature is not sufficiently high. Here we will show Near-edge X-ray absorption fine structure (NEXAFS) and X-ray photoelectron spectroscopy (XPS) data for such preparations. Data were taken at ID32 and BACH beamlines of ESRF and Elettra synchrotrons, respectively.

X-ray absorption spectroscopy (normal to the field and light incidence) for a approx. 1 ML thick Eu film deposited at a $T = 770$K hot hBN/Pt(111) substrate (10 minutes) and successive exposure to air is shown in Fig. S1. The air exposure was carried out with the sample at room temperature during five minutes. After air exposure a strong transformation of the spectral shape towards tri-valent Eu configuration took place. Nevertheless, even after the air exposure experiment a small di-valent part is still present. In order to remove remaining air adsorbates, the sample was post-annealed in UHV to $T = 470$K during 10 minutes.

Fig. S2 represents X-ray photoemission data from BACH beamline taken at a photon energy $h\nu = 272$eV. The substrate temperature during Eu deposition for the data shown in Fig. S2 was $T = 470$K. The data set includes measurements of hBN/Pt(111) and two successive Eu intercalations, each for 10 min at a very low rate. The total Eu thickness was calculated from the Pt 4f intensity loss taking into account the mean free path of the electrons. The latter was extracted from the universal curve of the electron mean free path [1] and resulted in Eu thickness of 0.7 and 1.5Å for 10 and 20 min Eu deposition, respectively. In Fig. S2 one observes the spin orbit split $4f_{7/2}$ and $4f_{5/2}$ components of the Pt 4f core level. These are further split in the surface (S) and bulk (B) emissions indicated in the Figure. It is interesting to note that the
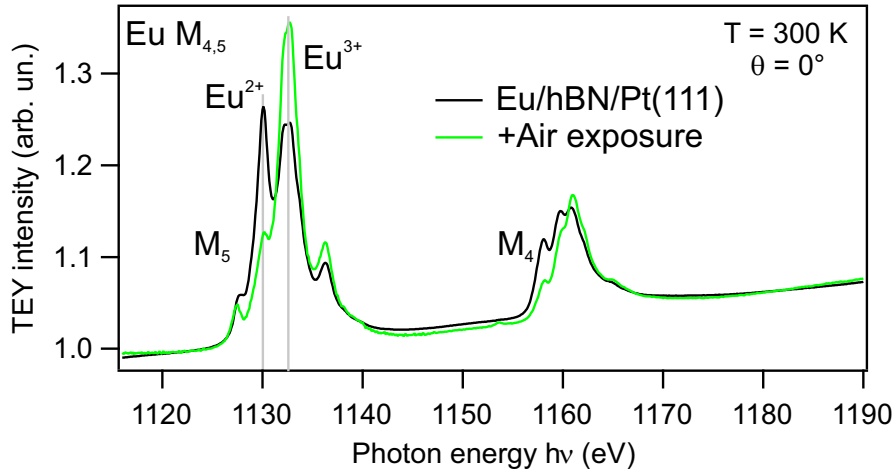

Figure S1. X-ray absorption spectra at the Eu $M_{4,5}$ absorption edge for Eu deposition on hBN/Pt(111) at $T = $ 770K and successive air exposure. Measurement carried out at room temperature and with the sample at normal incidence.
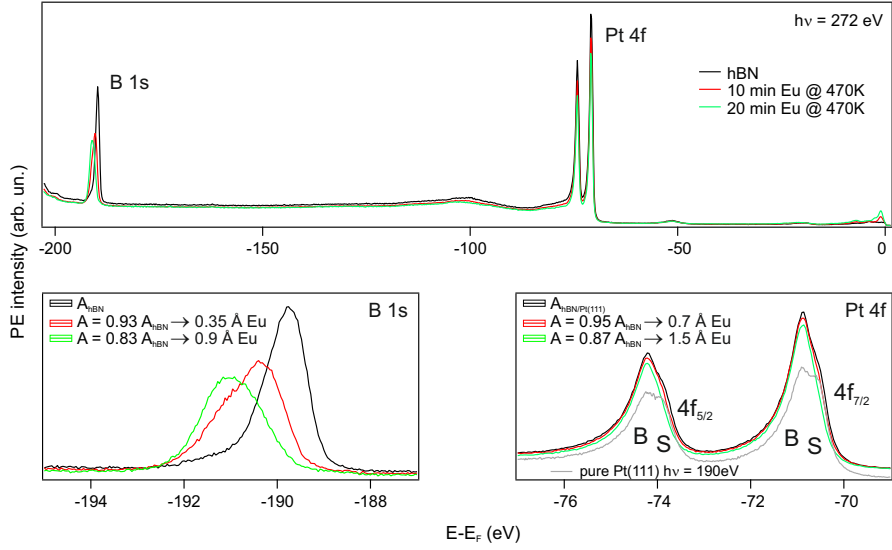
Figure S2. XPS analysis for sub-monolayer Eu deposition on hBN/Pt(111) at $T = 470$K. XPS survey, B 1s and Pt 4f emissions of 0.7 and 1.5Å Eu coverage on hBN/Pt(111), respectively, taken for $h\nu = 272$eV. In the case of the Pt 4f also the clean Pt emission is included to better observe the surface and bulk contributions ($h\nu = 190$eV). After low binding energy normalization, the areas A below the emissions were extracted and from them the overlayer amount was calculated by taking into account the electron mean free path of the electrons from the standard curve [1]. From this analysis we observe that not all Eu is intercalated below the hBN layer but rather stay on top.

surface emission can be still observed for hBN/Pt(111). This is possible due to the weak interaction of hBN and the Pt, specially at the (111) face that hosts a hBN Moire lattice. After Eu deposition the surface component shrinks much more than the bulk component, revealing that partial Eu intercalation occurred. We again calculate the Eu overlayer thickness but now from the B 1s core level that give us the amount of Eu on top of the hBN layer. The thickness that results from the area diminution is 0.35 and 0.9Å, respectively, for the two evaporations. This means that during the first deposition 0.35Å intercalated and after the second deposition 0.6Å out of the 1.5Å Eu intercalated. We also observe the doping effect of Eu towards the hBN layer that shifts the B 1s core level to higher binding energies in a similar way as for complete intercalation, see Fig. 6(a) of the main text.

The analysis of the valency has been carried out with resonant photoemission applying photon energies around the 4d→4f absorption edge. The results can be found in Fig. S3. At off-resonant photoemission ($h\nu = 132$eV) the Eu 4f emission is strongly suppressed, therefore the valence band is dominated by Pt 5d valence band emission. Nevertheless, there is already some Eu 4f emission. The 4f emissions are much better observed for the resonant photon energies $h\nu = 140$eV and 144.5eV corresponding to Eu^{2+} and Eu^{3+} resonances, respectively [2, 3, 4]. The di-valent emission is located at approx. 1.1eV binding energy, the tri-valent multiplet is observed between
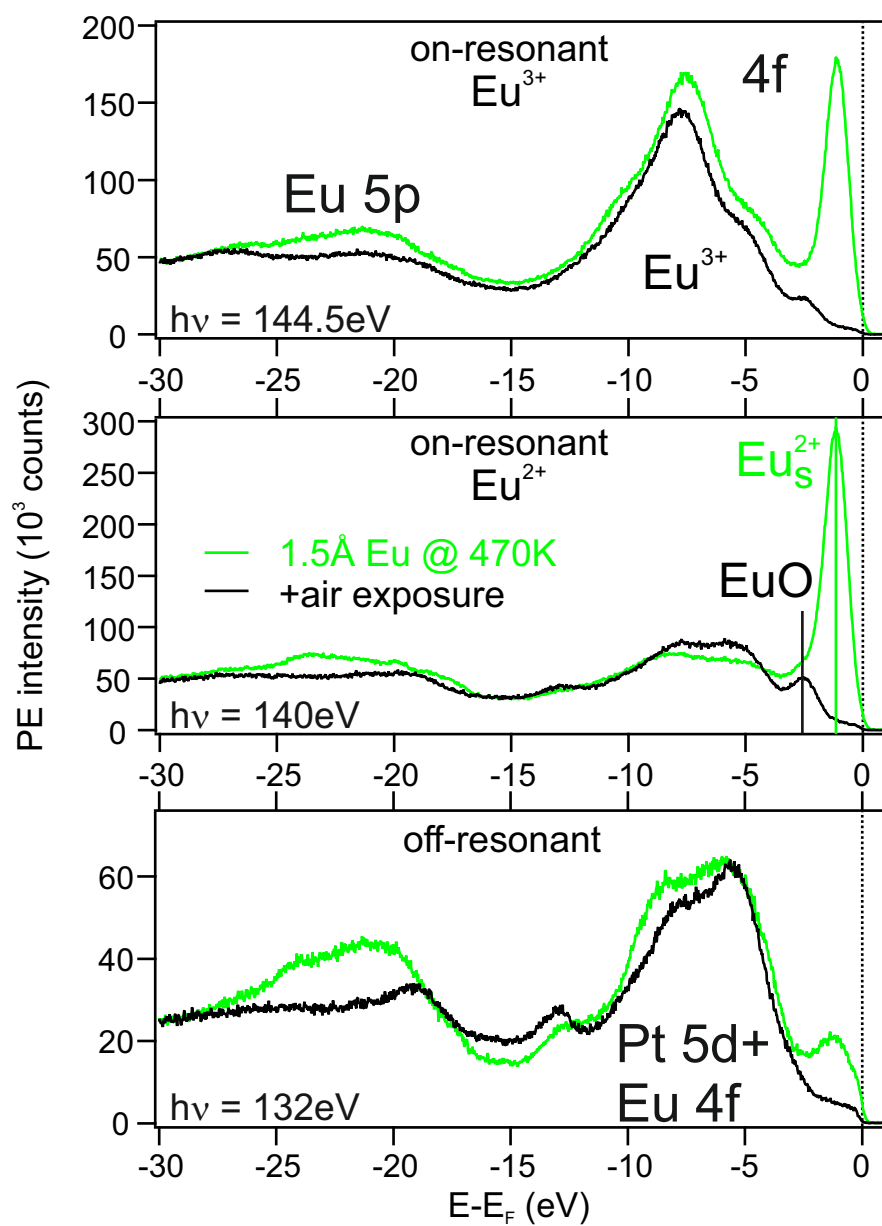
Figure S3. Resonant Photoemission at the Eu 4d→4f absorption edge.
Normal emission photoemission spectra of the valence band region of 1.5Å Eu deposited onto a 470K hot hBN/Pt(111) surface for three photon energies corresponding to off, on-resonant Eu^{2+}, and on-resonant Eu^{3+} at $h\nu = 132$, 140, and 144.5eV, respectively. Shown are spectra prior and after exposure of the sample to ambient conditions (5 min, room temperature).
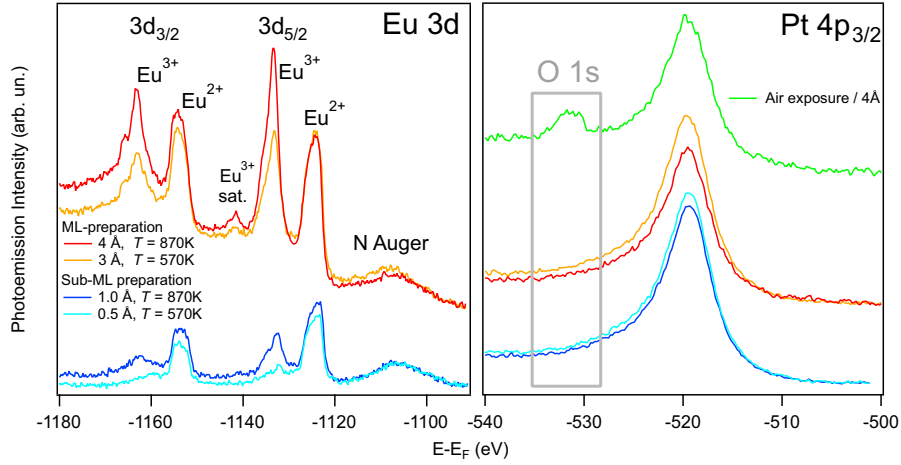
Figure S4. Additional X-ray photoemission spectra. Eu 3d, Pt $4p_{3/2}$ and O 1s emissions of the XPS series shown in Fig. 3 of the main text.

4 and 12eV. Due to the unknown cross-section effects around the resonances an exact Eu^{2+}/Eu^{3+} ratio cannot be extracted. The tri-valent contribution arises from a part of the intercalated Eu atoms that diffuse further inside the Pt bulk, but can also arise from oxidation of Eu to tri-valent Eu in Eu_2O_3 of the Eu atoms atop of the hBN layer. The latter oxidation is very difficult to avoid due to the strong reactivity of Eu even under very good ultra-high vacuum conditions [5]. After air exposure, the situation changes drastically. There is still a small di-valent signal, but now at a binding energy of 2.3eV. This Eu^{2+} emission cannot arise from di-valent Eu surrounded by a metallic environment whose binding energy is always lower than 2eV. But an emission at such 2.3eV arises from divalent Eu in EuO at surfaces [6, 3]. This oxide is usually unstable under ambient conditions but seems to be able to form and remain stable under used experimental conditions. EuO is created either on the surface or at the interface under hBN (and stabilized thanks to the interface). Further investigations would be necessary to distinguish both possibilities. In any case, we do not observe a possible divalent $EuPt_2$ structure below the hBN after the air exposure process for Eu deposition at 470K substrate temperature.

S2. Additional XPS data for Eu intercalation and air exposure

In Figs. S4, S5, and S6 we present additional XPS spectra for the preparations corresponding to Fig. 3 and 6(a) of the main text, respectively. In Fig. S4 the Eu 3d spectra of the main text is repeated with its corresponding O 1s emissions. Aim of this figure is to verify that the tri-valent emissions of the Eu 3d core level are not associated to a possible formation of the Europium oxide Eu_2O_3 since no O 1s emissions are observed prior to air exposure. This is indicated in the second panel of the figure that combines the Pt $3p_{3/2}$ and O 1s emissions that are close in energy but easily separable. For comparison, we add the spectra of the 4Å Eu spectrum after air exposure to indicate
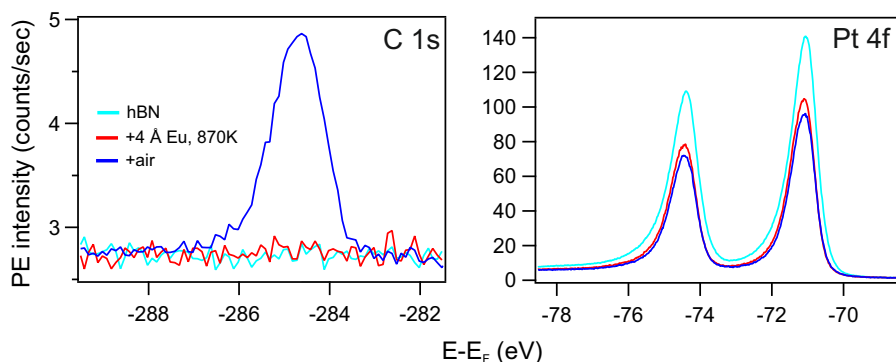
Figure S5. Additional X-ray photoemission spectra. C 1s and Pt 4f emissions of the XPS series shown in Fig. 6(a) of the main text.

the energy range of O 1s emissions due to the oxide and hydroxide formation that happen at ambient pressure.

Furthermore, in Figs. S5 and S6 the C 1s and Pt 4f emissions as well as peak fit results of the N 1s core level spectra of Fig. 6(a) of the main text are shown. Eu deposition and additional air exposure cause that the Pt 4f core level reduces accordingly. After air exposure, an additional C 1s emission is observed that is assigned to adventitious C 1s (saturated hydrocarbons) [7]. From the intensity loss of the N Auger and Pt 4f emissions and by taking into account the cross sections and surface sensitivity of the XPS spectrum we estimate the hydrocarbon overlayer thickness to roughly 0.5nm after air exposure and annealing. This damping also affects the Eu^{2+} emission that lowered to 1/3 of its original intensity but by taking into account the mentioned damping means that only half of the original Eu^{2+} signal is lost.

Additionally, the N 1s photoemission was further considered by peak fit procedures and the results are presented in Fig. S6. For this purpose, Doniach-Šunjic lineshapes have been employed and a linear background that accounts for the secondary electron emissions from the Au 4d peaks nearby. The leading peak position was observed at 397.2eV binding energy by Preobrajenski et al. [8], at 397.3eV by Nagashima et al. [9], and we obtain 397.4eV. In a second step we fit the N 1s spectrum after Eu intercalation. We see that in this case we can fit rather well the spectrum with 3 emissions, one corresponding to the doublet found for the clean case, and two additional Doniach-Šunjic lines at binding energy positions 398.5eV and 399.3eV with a rather similar width and intensity. The latter peak positions and splitting resamples the situation for hBN/Rh(111) with positions 397.9eV and 398.6eV [8] but shifted now by approx. 0.6eV to higher binding energy. The hBN/Rh(111) system - called nanomesh - has a stronger interaction as hBN/Pt(111) leading to a core level shift to higher binding energy and to a much stronger pronunciation of the two peaks that are assigned to emissions from nitrogen atoms with a stronger (high binding energy) and weaker (lower binding energy peak) interaction with the Rh substrate. This situation results from the position of the N atom inside the nanomesh caused by the lattice mismatch between hBN and
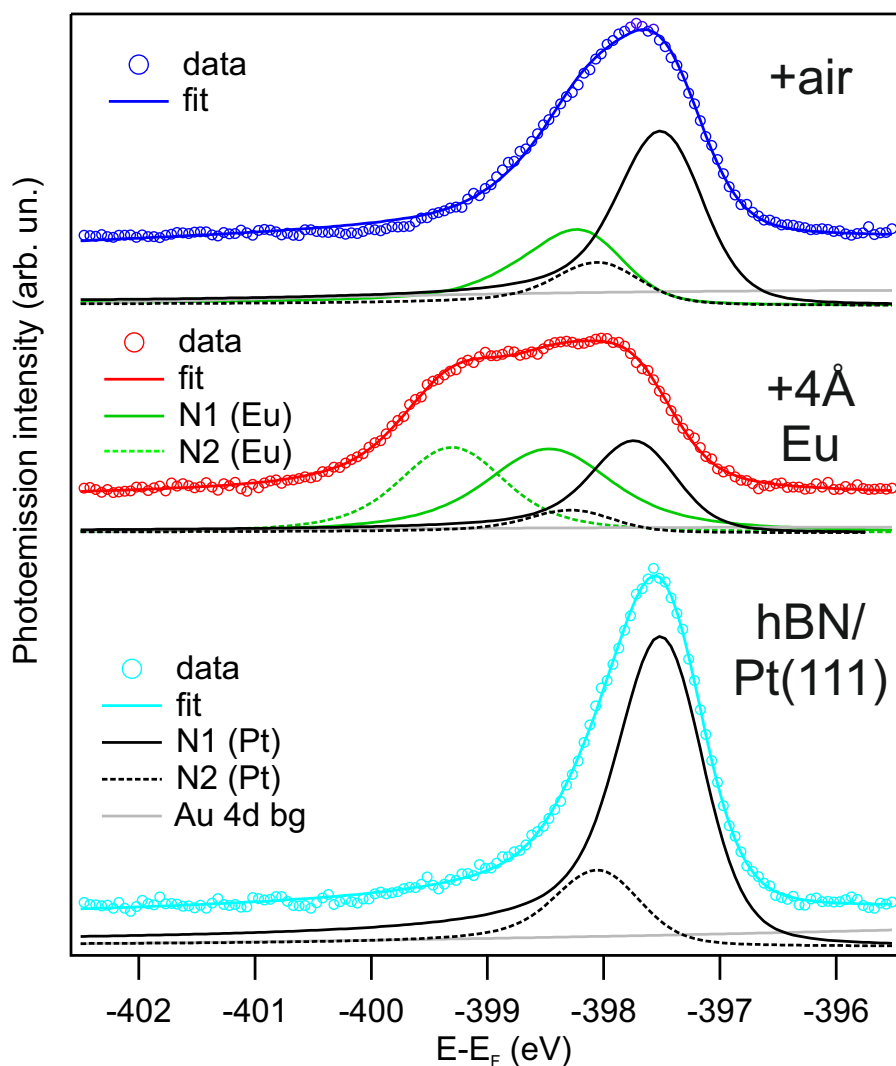
Figure S6. Additional X-ray photoemission spectra. N 1s core level fits for pure hBN/Pt(111), with 4Å Eu intercalated at 870K and after air exposure and annealing. The fits correspond to the data presented in Fig. 6(a) of the main text.

Rh. In the here considered case of hBN/EuPt$_2$ we observe an even stronger interaction and therefore obtain an even larger binding energy and an even stronger second peak emission. From the XPS fit we also observe that approx. 1/3 of the sample is still Eu free. This means that intercalation, although completed from the point of view that all Eu is below the hBN is not enough to get an alloy everywhere at the interface. After exposure to air, the picture change, Eu gets partially oxidized, partially the di-valent character is preserved. This behaviour results in the disappearance of the very strong interaction peak, a similar less interacting nitrogen peak on Eu, and an increase of the very weak interacting peak that was found initially for hBN/Pt(111). hBN on oxidized europium is very likely to interact weakly in a similar way as hBN on Pt, therefore the latter emission may include such hBN areas on europium oxide.
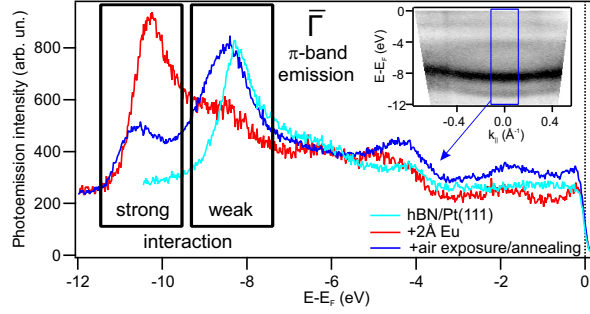
Figure S7. Additional valence-band photoemission results. π-band emission of hBN at the $\bar{\Gamma}$-point of the surface Brillouin zone of clean hBN/Pt(111), 4Å Eu intercalated below hBN at 870K, and after air exposure and successive annealing, respectively. Photon energy of the measurement was 40.8eV (HeII emission), measurement temperature 300K. The inset shows the ARPES intensity close to the $\bar{\Gamma}$-point along $\bar{M}\bar{\Gamma}\bar{M}$ direction after air exposure.

S3. Additional ARPES data for Eu intercalation and air exposure

To further observe the influence of the air exposure in ARPES data, in Fig. S7 the angle-resolved photoemission spectra at the $\bar{\Gamma}$-point of the surface Brillouin zone is presented for clean hBN/Pt(111), 4Å Eu intercalated below hBN at 870K, and after air exposure and successive annealing. For better statistics the angular integration range has been set to ±3°. Initially, the π-band for hBN/Pt(111) is found 8.3eV below the Fermi level. Intercalation of 4Å Eu leads to a nearly complete disappearance of the hBN/Pt(111) π-band and the appearance of a new π-band at 10.3eV below the Fermi level corresponding to a strongly interacting hBN layer on $EuPt_2$. Air exposure and further annealing to remove the rest-air contamination change again the π band structure. One now observes two π-bands (see inset for dispersion along $\bar{M}\bar{\Gamma}\bar{M}$ direction), the one at higher binding energy has lost intensity and is again attributed to the hBN on the remaining not-oxidized $EuPt_2$ patches while the lower binding energy branch is interpreted as a superposition of bands arising from hBN on the oxidized part and from clean Pt(111) areas, where the Eu intercalation did not take place. The band minimum of the weakly interacting π-band is now at 8.5eV below the Fermi level. This means that the energy positions of the π-band on hBN/Pt and on the oxide part are slightly different but too close to be able to be separated in our measurements.

S4. Additional magnetization measurements, magnetic anisotropy determination

In Fig. S8(a) we repeat the X-ray absorption spectra of Fig. 5(a) of the main text but add now the XMCD spectrum after removing the applied field keeping the sample in remanence. Although the XMCD signal has dropped considerably (to 4% of the 6T spectrum), the remanence XMCD spectrum still reveal the same shape as for the applied field. This is proof of the ferromagnetic behaviour of the $EuPt_2$ magnetic layer.
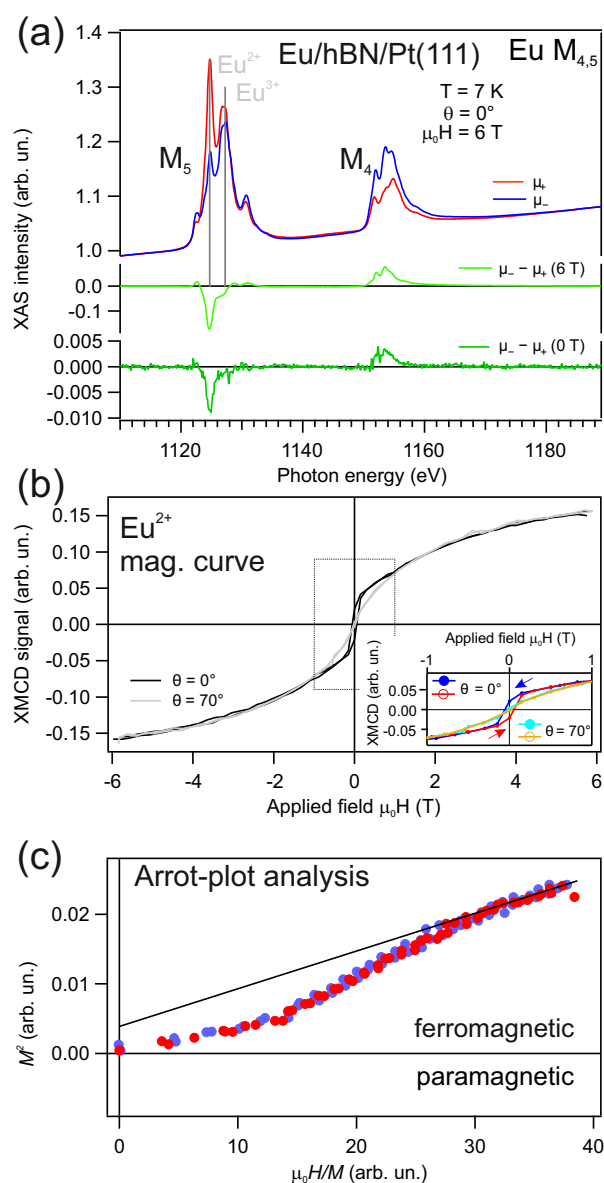
Figure S8. Additional XMCD results of Eu. (a) XAS and XMCD at the Eu $M_{4,5}$ absorption edge in normal incidence geometry. The XMCD difference spectra for 6T and at remanence (applied field 0T) are shown. (b) Eu magnetization curves normal and at $\theta = 70°$ with respect to the field. The inset shows a closeup at small fields to distinguish better the two curves. One clearly observes the more rectangular like shape for the out-of-plane geometry revealing an out-of-plane easy axis. (c) Arrot plot analysis [10] of the normal incidence geometry magnetization curve. The black line presents a linear fit to the high-field (high $\mu_0 H/M$ values).

The magnetic anisotropy of the intercalated Eu can be determined from the two different geometries applied. The magnetization curves for the sample perpendicular and at an angle of 70° with respect to the applied field is shown in Fig. S8(b). The close-up at small fields reveal a more rectangular shape of the out-of-plane geometry magnetization loop pointing to this direction as the easy axis of magnetization. The XMCD values close to zero-field has been taken from individual complete XMCD measurements to avoid the typical zero-field artifacts of XMCD measurements.

Fig. S8(c) reveal the Arrot plot analysis [10] of the normal incidence magnetization curve (applied field normal to the sample). This analysis confirms the ferromagnetic state of the $EuPt_2$ surface alloy. In such analysis, the square of the magnetization M^2 is plotted against the applied field divided by the magnetization $\mu_0 H/M$. A linear fit of the high field (high $\mu_0 H/M$) values indicates ferromagnetic state if the line hits the ordinate at a positive M^2 value, and paramagnetism if the ordinate crossing is negative. For the fit the XMCD values between +5T and +6T and between -5T and -6T have been used.

[1] Dench W A and Seah M P 1979 Quantitative Electron Spectroscopy of Surfaces: A Standard Data Base for Electron Inelastic Mean Free Path in Solids *Surf. Interf. Anal.* **1** 1

[2] Schneider W D, Laubschat C, Kalkowski G, Haase J and Puschmann A 1983 Surface effects in eu intermetallics: A resonant photoemission study *Phys. Rev. B* **28** 2017–2022

[3] Santana J A C, Liu P, Wang X, Tang J, McHale S R, Wooten D, McClory J W, Petrosky J C, Wu J, Palai R, Losovjy Y B and Dowben P A 2012 The local metallicity of gadolinium doped compound semiconductors *Journal of Physics: Condensed Matter* **24**(44) 445801

[4] Banik, Soma and Bendounan, Azzedine and Thamizhavel, A and Arya, A and Risterucci, P and Sirotti, F and Sinha, A K and Dhar, S K and Deb, S K 2012 Electronic structure of eucu$_2$ge$_2$ studied by resonant photoemission and x-ray absorption spectroscopy *Phys. Rev. B* **86** 085134

[5] Schumacher S, Huttmann F, Petrović M, Witt C, Förster D F, Vo-Van C, Coraux J, Martínez-Galera A J, Sessi V, Vergara I, Rückamp R, Grüninger M, Schleheck N, Meyer zu Heringdorf F, Ohresser P, Kralj M, Wehling T O and Michely T 2014 Europium underneath graphene on Ir(111): Intercalation mechanism, magnetism, and band structure *Phys. Rev. B* **90** 235437

[6] Caspers C, Müller M, Gray A X, Kaiser A M, Gloskovskii A, Fadley C S, Drube W and Schneider C M 2011 Chemical stability of the magnetic oxide euo directly on silicon observed by hard x-ray photoemission spectroscopy *Phys. Rev. B* **84** 205217

[7] Barr T L and Seal S 1995 Nature of the use of adventitious carbon as a binding energy standard *Journal of Vacuum Science & Technology A* **13**(3) 1239–1246

[8] Preobrajenski A B, Vinogradov A S, Ng M L, Ćavar E, Westerström R, Mikkelsen A, Lundgren E and Mårtensson N 2007 Influence of chemical interaction at the lattice-mismatched h-BN/Rh(111) and h-BN/Pt(111) interfaces on the overlayer morphology *Phys. Rev. B* **75** 245412

[9] Nagashima A, Tejima N, Gamou Y, Kawai T and Oshima C 1995 Electronic structure of monolayer hexagonal boron nitride physisorbed on metal surfaces *Phys. Rev. Lett.* **75** 3918–3921

[10] Arrott A 1957 Criterion for ferromagnetism from observations of magnetic isotherms *Phys. Rev.* **108** 1394–1396